

RL over Commodity Networks: Overcoming the Bandwidth Barrier with Lossless Sparse Deltas

Chaoyi Ruan¹ Geng Luo¹ Xinyi Wan¹ Long Zhao² Qinghe Wang²
 Jian Zhu³ Duling Xu⁴ Guanbin Xu⁵ Dehui Wei¹ Xiang Liu¹
 Cheng Li³ Haifeng Sun¹ Congcong Miao¹ Jialin Li¹

¹*NUS* ²*Anhui University* ³*USTC* ⁴*Renmin University of China* ⁵*Unaffiliated*

ABSTRACT

LLM post-training with reinforcement learning (RL) requires frequent synchronization of large model parameters between the trainer and distributed rollout actors. High-throughput RL post-training therefore relies on dedicated RDMA HPC clusters, an infrastructure cost most organizations cannot absorb. A natural alternative is to aggregate loosely-coupled GPUs over standard Ethernet and WAN links, but this commodity connectivity cannot sustain full-weight broadcasts: synchronizing an 8B model can take over 100 seconds on bandwidth-limited links, while rollout generation typically takes tens of seconds.

Toward making RL practical in this regime, we observe that RL fine-tuning yields highly sparse per-step updates, with only around 1% of parameter elements changing. Atop this insight, we present SparrowRL, a novel high-performance RL training system that preserves bit-exact updates without dropping or quantizing information, designed for commodity-networked, loosely-coupled GPU resources. SparrowRL represents each step as a sparse delta checkpoint, pipelines delta extraction with multi-stream transmission, overlaps transfer with rollout generation, and coordinates heterogeneous workers with throughput- and bandwidth-aware scheduling plus lease-based fault tolerance. On Qwen3 models from 4B to 14B deployed across up to four geographic regions, SparrowRL reduces per-step transfer payload by 79× for Qwen3-8B and improves throughput by 2.4–9.5× over full-weight broadcast across WAN, narrowing the throughput gap relative to an ideal RDMA single-datacenter baseline to within 8.91%. By leveraging on-demand, cross-cloud GPUs over commodity links, SparrowRL delivers 1.21–1.59× higher tokens per dollar than reserved RDMA clusters at comparable throughput.

1 INTRODUCTION

Reinforcement learning (RL) has emerged as a critical post-training paradigm for large language models (LLMs), with

systems such as DeepSeek-R1 [14] and GPT-4o [36] demonstrating that RL can unlock strong reasoning capabilities. RL post-training follows a trainer-actor architecture in which a Trainer updates the policy and refreshes Rollout Actors, which generate samples and return them for training (Figure 1). In this workflow, the additional transfer of updated parameters to Rollout Actors becomes a potential bottleneck for end-to-end throughput. Because RL requires a full-weight refresh at every training step, as the model size grows, this transfer overhead increasingly dominates the iteration time and leaves the compute resources idle while waiting for the next policy version.

State-of-the-art RL systems assume RDMA-connected GPU HPC clusters as the default deployment model, which we refer to as *tightly-coupled clusters*. In these clusters, RDMA fabrics and co-located scheduling make per-step synchronization across the Trainer and Actors fast and predictable. The design of existing RL frameworks is fundamentally based on high-bandwidth RDMA fabrics as the backbone.

In contrast, *loosely-coupled deployments* aggregate on-demand GPU resources across multiple cloud providers, university labs, or geographic regions [27, 51] via commodity networks. Enabling efficient RL training on this infrastructure would democratize access to frontier research, allowing academic groups and startups to work on large-scale models without the prohibitive costs and exclusivity of dedicated HPC clusters. The key constraint for such configurations, however, is network connectivity: cross-region and cross-provider links typically offer only 1–10 Gbps bandwidth and exhibit high WAN latency and loss rate [27].

Existing RL system designs are poor fit for commodity networks because they couple training progress with frequent dense broadcasts and fine-grained coordination. Loosely-coupled deployments face two fundamental challenges: (1) the *commodity network barrier*, where limited bandwidth and high jitter stall both data movement and control loops, and (2) *heterogeneity and instability* from variable node throughput and preemption. Prior RL systems such as OpenRLHF [18],

Chaoyi Ruan and Geng Luo equally contributed to this work.

veRL [43], and StreamRL [54] optimize rollout efficiency, but rely on high-bandwidth intra-cluster networks. When these RL systems are ported to a commodity network, the full weight broadcast achieves low effective throughput, causing the synchronization of a small 8B model to take over 100 seconds (Table 2), far exceeding the time required for rollout generation, and driving GPU utilization into single digits.

Optimizing distributed RL on commodity networks requires a fundamental shift in design principles. Rather than treating the RL training loop as a *black box* and relying solely on high-bandwidth hardware to brute-force expensive synchronization, we argue for a *white box* approach that reveals the exploitable structures in RL workflows and co-designs system-level mechanisms with algorithmic insights.

Through extensive profiling across multiple model families and RL algorithms, we discover a critical property that makes bandwidth-efficient RL training feasible: *parameter updates are remarkably sparse*. Unlike pre-training, only 1–3% of parameter elements change per iteration, creating an opportunity to reduce transfer volumes by two orders of magnitude. This inherent sparsity fundamentally changes the bandwidth demand for distributed RL.

Inspired by this principle, we build SparrowRL, a novel RL training system designed for commodity-networked, loosely-coupled GPU resources, delivering high throughput and cost-efficiency without sacrificing accuracy. SparrowRL combines three co-designed mechanisms. First, it unifies checkpoint storage and network transfer into a single abstraction, the *lossless delta checkpoint*: each training step produces a versioned, immutable artifact that captures only the sparse parameter changes with full precision, using delta-encoded variable-length indexing to further compress position metadata beyond the base sparsity ratio. Second, a *streaming transfer protocol* pipelines delta extraction with cut-through forwarding over multiple parallel network streams and employs relay-based fanout to scale delivery across regions, while overlapping transfer with rollout generation so that Actors stage the next version behind ongoing computation. Third, *heterogeneity-aware scheduling* combined with *lease-based fault tolerance* coordinates loosely-coupled workers: the scheduler sizes each Actor’s batch in proportion to its observed throughput and link bandwidth so that all Actors complete within a one-step policy lag, while time-bounded leases detect failures implicitly and redistribute work without global barriers while preventing stale rollouts.

We implement SparrowRL atop FSDP2 [39] and vLLM [25] as high-throughput training and inference engines, requiring no modifications to the underlying RL algorithms. We evaluate SparrowRL on Qwen3 models from 4B to 14B across up to four geographic regions spanning North America, Europe,

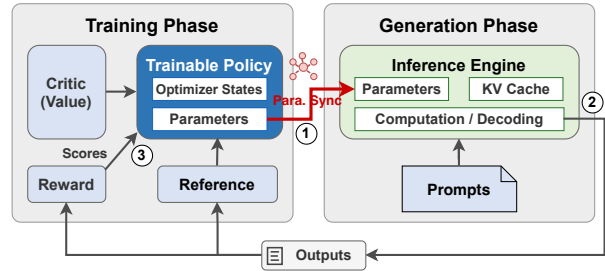


Figure 1: RL training architecture for LLMs. The Trainer holds the policy and auxiliary models; Rollout Actors generate rollouts from prompts. Updated weights are transferred every iteration.

and Asia-Pacific. SparrowRL reduces per-step transfer payload by 79× for Qwen3-8B and improves throughput by 2.4–9.5× over full-weight broadcast across WAN, narrowing the throughput gap relative to an ideal RDMA single-datacenter baseline to within 8.91%, down from 90.3% under full-weight broadcast. Leveraging cross-cloud GPUs over commodity links, SparrowRL achieves 1.21–1.59× higher tokens per dollar than RDMA clusters at comparable throughput.

2 BACKGROUND AND MOTIVATION

2.1 Reinforcement Learning for LLMs

Reinforcement learning has emerged as the standard paradigm for post-training LLMs, enabling capabilities beyond supervised fine-tuning [34, 44]. Most systems follow a training-generation workflow (Figure 1) that tightly couples a Trainer with a set of Rollout Actors. Each step comprises three actions: ① the Trainer synchronizes the updated policy parameters π_t to the Rollout Actors, ② the workers generate rollout samples from prompts and return trajectories, and ③ the Trainer computes rewards and advantages using the reward model and critic, then updates the policy to produce π_{t+1} . In this workflow, parameter transfer is on the critical path of each step. To mitigate this cost, recent systems adopt one-step asynchronous RL [11, 35, 54], where the generation at step $t+1$ proceeds with stale weights π_t while the Trainer computes π_{t+1} in parallel. This shifts synchronization off the critical path by overlapping it with generation, provided that the transfer completes within one generation period.

Although rollout samples returned from generation to training are very small, weight transfer incurs a high communication cost. Even an 8B model in BF16 requires sending approximately 16 GB to *each* Rollout Actor per step, and this cost scales linearly with model size.

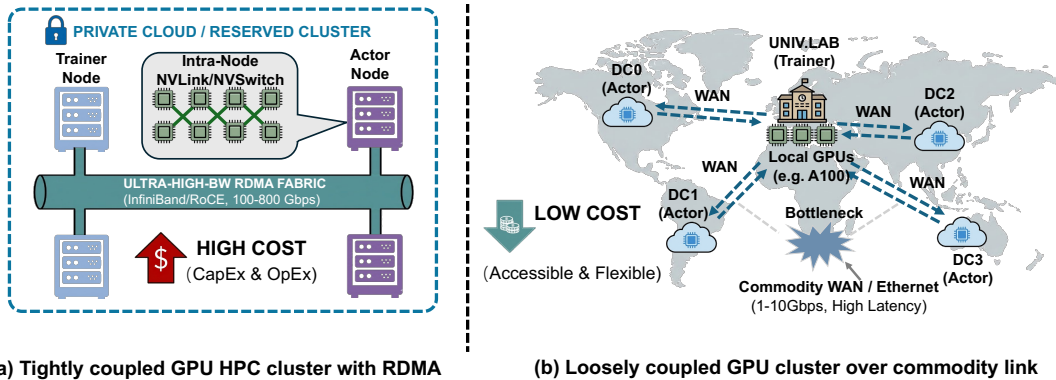


Figure 2: Two paradigms for RL training. Left: tightly coupled clusters with RDMA interconnects (100–800 Gbps) and high cost. Right: loosely coupled resources across labs and clouds, connected via cross-cloud links (1–10 Gbps).

Table 1: Cost and accessibility trade-offs for renting a 16-GPU deployment: RDMA clusters typically require long minimum commitments and sales-team approval at scale, whereas cross-cloud configurations can stitch together on-demand, flexible capacity across providers.

Configuration (Provider)	\$/hr (Min. Commit)	BW
<i>Tightly coupled (RDMA fabric)</i>		
2×8×H100 w/ EFA (AWS)	32 (24 hr, reserved)	3.2 Tbps
2×8×H100 w/ IB (Lambda)	38 (1 week, reserved)	3.2 Tbps
<i>Loosely coupled (cross-cloud)</i>		
8×H100 (Hyperbolic [19]) + 8×H100 (Hyperstack [20])	27 (1 hr, on-demand)	1 Gbps
8×H100 (Hyperbolic [19]) + 8×A100 (Lambda [26])	26 (1 hr, on-demand)	1 Gbps

2.2 The HPC-Centric Status Quo

State-of-the-art RL systems assume RDMA-connected HPC clusters as the default deployment model, as illustrated in Figure 2-(a). With high-end RDMA fabrics and co-located scheduling, a full-weight refresh completes in roughly one second (Table 2). For example, Perplexity [37] reports similar sub-2 s transfers in RL post-training deployments, so existing designs treat per-step synchronization as a small overhead.

This infrastructure requirement introduces both cost and access barriers (Table 1). RDMA clusters typically charge a network premium over commodity Ethernet, for example \$39/hour versus \$31/hour for 16×H100 on Hyperbolic, which is a 26% increase [19]. Providers also gate these clusters behind minimum reservations, so an exploratory 48-hour run can become a one-week commitment that inflates cost by 3.5×. Beyond cost, access remains constrained. Academic institutions, government labs, and small organizations often lack the procurement relationships or credit lines needed to reserve large GPU blocks. The result is that high-bandwidth RL training remains concentrated among well-funded industry labs, while the broader research community and small companies face substantial infrastructure barriers to entry.

Table 2: Impact of network bandwidth on full-model synchronization for Qwen3-8B (16 GB in FP16).

Network	Trainer	Actor	BW	Sync
HPC fabric (RDMA)			100 Gbps	1.3 s
Commodity network	40 s	45 s	1 Gbps	128 s

2.3 Loosely Coupled GPU Resources: Opportunity and Challenges

Commodity networks: an accessible alternative. RL post-training has become a common step for adapting LLMs, and it attracts users beyond the few organizations that can run large-scale pretraining, including academic labs and small companies. Many of these users can access GPUs, but they cannot access a large, single RDMA-connected cluster at scale. Commodity networks offer an accessible alternative by connecting GPUs over standard Ethernet and WAN links rather than dedicated RDMA fabrics, as illustrated in Figure 2-(b). In practice, we increasingly see three common scenarios: (1) heterogeneous instances within a single cloud, where training and generation run on different GPU types that communicate over commodity networking (well below RDMA fabrics) [29, 47, 54], (2) cross-region or multi-cloud RL training that aggregates on-demand GPUs when no single region offers sufficient capacity [10, 17], for example from AWS, Lambda, and GCP [3, 13, 26], and (3) cross-institution collaborations that pool GPUs across labs [5, 40]. Commodity networks aggregate GPU capacity across providers and offer a more economical on-demand deployment option.

As shown in Table 1, for a 16-GPU setup, RDMA-connected H100 clusters cost \$32–\$38 per hour and typically require 24 hours to one week of minimum commitment, while combining 16 GPUs from two on-demand providers costs \$26–\$27 per hour with 1-hour billing. The savings come with weaker

Table 3: Comparison of RL system capabilities for geo-distributed deployment. \circ : partial support with significant trade-offs.

Architecture	Example system(s)	C1	C2
Colocated	OpenRLHF [18], veRL [43]	\times	\times
Disaggregated	StreamRL [54]	\times	\circ
Decentralized	PrimeRL [45]	\times	\checkmark
Sparse-delta	SparrowRL	\checkmark	\checkmark

connectivity, where commodity links provide 1–10 Gbps rather than multi-terabit RDMA fabrics. This connectivity gap is precisely what SparrowRL targets by making these deployments practical for RL post-training. We formalize the resulting constraints as Challenges 1–2 below.

Challenge 1 (C1): the commodity network barrier. Commodity WANs impose two sources of penalty on distributed training: limited bandwidth throttles data movement, while high latency stalls workflow loops. First, full model weight transfer dominates iteration time on bandwidth-limited links. At datacenter-grade bandwidths (100+ Gbps), weight transfer constitutes a minor fraction of each iteration. However, on 1–10 Gbps WAN links, transfer time increases rapidly and stretches the critical path. As shown in Table 2, transferring a 16 GB model takes more than 100 s on a 1 Gbps link, limiting throughput regardless of GPU speed. On HPC fabrics, the 1.3 s transfer fits easily within the 45 s generation window, but on a commodity link, the 128 s transfer exceeds the entire generation period, so even one-step asynchronous RL cannot fully hide the transfer cost. Second, inter-region RTTs (tens to hundreds of milliseconds) are higher than sub-millisecond datacenter fabrics [32], adding visible latency to the small control messages exchanged at each step.

Challenge 2 (C2): heterogeneity and failures. Cross-cloud deployments aggregate nodes with substantial variation in both compute capacity and reliability. GPU instances range from older L40 and A100 GPUs to newer H100 hardware, with generation throughput differing by 2 to 3 \times . Network conditions are equally heterogeneous and more unstable: Actors from nearby providers may achieve 5 to 10 Gbps bandwidth to the Trainer, while those across continents operate at 1 to 3 Gbps. Beyond static heterogeneity, these deployments experience dynamic disruptions due to instance failures, and stragglers resulting from thermal throttling or resource contention.

Why do existing systems fall short? We classify existing works into three architectural categories (Table 3). (1) **Colocated architectures** (OpenRLHF [18], veRL [43]) couple generation and training on the same nodes, relying on

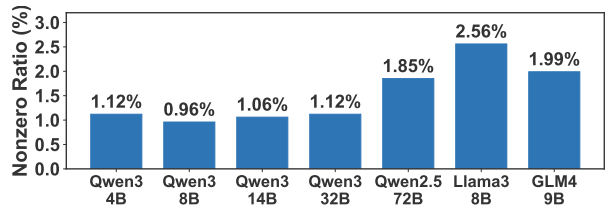


Figure 3: Fraction of nonzero parameter updates after one RL step across different models.

Table 4: Fraction of nonzero parameter updates after one RL step for Qwen3-8B under different algorithms.

Algorithm	GRPO [41]	RLOO [2]	OPO [15]
Nonzero Ratio ρ (%)	0.96	0.93	1.06

high-bandwidth datacenter fabrics (failing C1/C2). (2) **Disaggregated architectures** (StreamRL [54]) separate generation and training clusters to handle heterogeneity, but rely on high-bandwidth dedicated links (e.g., 80 Gbps) for state transmission, remaining bound by the network barrier (C1). (3) **Decentralized architectures** (PrimeRL [45]) decouple Actors fully for internet-scale deployment (C2), but still transfer full model weights, suffering from the same bandwidth bottleneck (C1). To compensate, they rely on multi-step parameter staleness between training and inference to hide the transfer cost, which compromises model quality.

SparrowRL bridges this gap by exploiting RL-specific sparsity to compress weight transfers, enabling one-step asynchronous RL to fully hide synchronization cost even over commodity networks, thereby addressing both challenges without sacrificing model accuracy.

3 KEY INSIGHT AND DESIGN PRINCIPLES

The challenges in § 2.3 appear fundamental if we treat the RL system as a monolithic black box. However, by dissecting the RL workflow, we uncover a critical property: *parameter update sparsity*. This property, combined with the structural independence of RL tasks, allows us to transform network bottlenecks into design opportunities. We propose three principles to address the identified challenges.

Empirical basis: fine-grained sparsity. We first quantify parameter changes in a single RL step. An LLM consists of K parameter tensors $\{W^{(k)}\}_{k=1}^K$ (e.g., attention projections and MLP weights). Let $W_t^{(k)}$ and $W_{t+1}^{(k)}$ denote the values of tensor k before and after one RL step, and define the element-wise difference $\Delta W^{(k)} = W_{t+1}^{(k)} - W_t^{(k)}$ obtained by

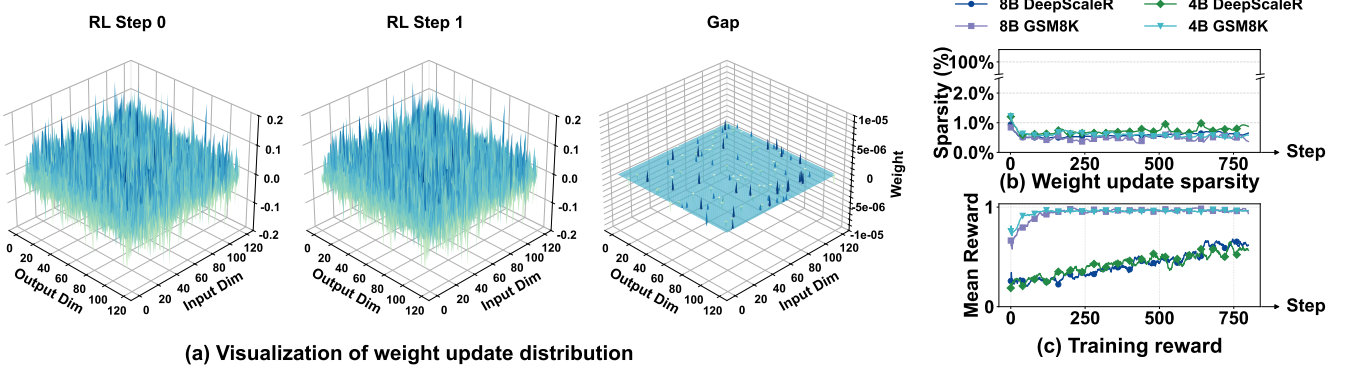


Figure 4: Analysis of training dynamics. (a) Visualization of weight update distribution, demonstrating the sparse nature of parameter updates. (b) Weight update sparsity and (c) training reward throughout RL training. We train 4B/8B models on GSM8K [8] and DeepScaleR [31] datasets for 800 rollout steps with a fixed learning rate of 1×10^{-6} .

differencing consecutive checkpoints. We define the element-wise *nonzero ratio* ρ across the entire model as

$$\rho = \frac{1}{\sum_{k=1}^K |W^{(k)}|} \sum_{k=1}^K \|\Delta W^{(k)}\|_0 \quad (1)$$

where $|W^{(k)}|$ is the number of scalar parameters in tensor $W^{(k)}$ and $\|\cdot\|_0$ counts nonzero elements. Crucially, this sparsity is fine-grained: while almost every tensor in the model receives updates, only a tiny subset of elements within each tensor changes, as shown in Figure 4-(a). This ratio is consistently low across different model families and under different RL algorithms. For instance, Figure 3 shows that for Qwen3-4B, only 1.12% of parameters change after an update. Similar nonzero ratios are observed for larger models such as Llama3-8B (2.56%), GLM4-9B (1.99%), and Qwen2.5-72B (1.85%). In addition, Table 4 shows that, when measured on Qwen3-8B, RL algorithms like GRPO [41], RLOO [2], and OPO [15] all modify around 1% of parameters per step.

Importantly, this sparsity is uniformly distributed across all weight tensors: every layer receives updates, but only a small fraction of elements within each tensor are modified. This pattern is not coincidental but arises from fundamental properties of RL fine-tuning. The learning rate for post-training alignment is on the order of 10^{-6} [24, 30, 50], two orders of magnitude below the 10^{-4} rates used in pre-training [9, 28], enabling behavioral refinement while preserving foundational knowledge. Recent theoretical work attributes this behavior to RL’s in-distribution nature: online updates are more robust to forgetting and naturally induce smaller parameter changes than supervised approaches [33, 42]. Regularization techniques including KL divergence constraints and gradient clipping [52] further bound update magnitudes. Crucially, this sparsity is a persistent property rather than a transient artifact: as shown in Figure 4-(b-c),

the update ratio remains stable throughout training, rapidly falling below 1% and staying there across 800 steps.

Driven by this empirical insight and the structural properties of RL workflow, we propose three design principles to explore new RL opportunities.

Principle 1: Make fine-grained sparsity a first-class primitive. Fine-grained sparsity makes full weight transfer unnecessary. Instead, the Trainer extracts a *fine-grained sparse delta* and synchronizes only the changed elements, typically $\sim 1\%$ of parameters as shown in Figure 3, while preserving bit-exact parameter updates.

Beyond bandwidth, WAN latency and actor heterogeneity also limit throughput. We thus leverage the *decomposability* of sparse updates and the *independence* of rollout tasks.

Principle 2: Streaming, pipelining, and overlap. Sparse updates are *decomposable*, so we stream the delta in segments while it is extracted and pipeline segment transfer with rollout generation. This overlap hides WAN latency (C1) and avoids file-level synchronization stalls.

Principle 3: Elastic task scheduling. Rollout generation is *task independent*, so we schedule tasks at rollout granularity. This elasticity tolerates actor failures and speed heterogeneity (C2) without global stalls.

4 OVERVIEW OF SPARROWRL

We propose SparrowRL, an RL training system for LLMs that exploits the inherent sparsity of policy updates to operate efficiently over commodity networks, addressing two barriers absent in datacenter fabrics (§ 2.3). Figure 5 illustrates the resulting architecture.

Deployment model. SparrowRL targets a deployment where a centralized Trainer runs on a well-provisioned cluster while inference capacity is distributed across multiple cloud providers or geographic regions. As shown in Figure 5,

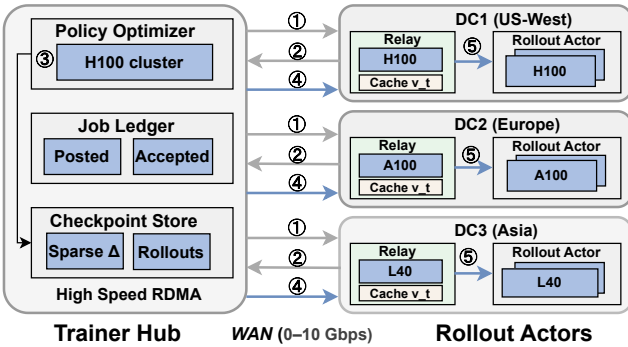


Figure 5: SparrowRL architecture overview. The Trainer Hub posts jobs and sparse deltas; Rollout Actors claim prompts, generate samples, and return results. Each region contains a Relay that receives deltas from the Trainer and forwards them to peer Rollout Actors.

the Trainer Hub connects to regional Relays over cross-cloud links up to 10 Gbps, depending on provider peering and network conditions. This model matches the actor-learner workflow common in LLM RL post-training: Actors generate rollouts while the Trainer updates the policy, and the system must tolerate stale Actors without stalling progress. By designing for bandwidth-constrained networks, SparrowRL handles cross-cloud deployments where academic groups and small organizations aggregate GPU capacity from multiple providers.

System components. The architecture comprises two logical tiers (Figure 5). The **Trainer Hub** serves as the coordinator for policy state. It runs the policy optimizer (e.g., GRPO) on a well-provisioned cluster (e.g., H100s) interconnected via high-speed RDMA fabric, maintains a **Job Ledger** tracking posted and accepted work, and operates a **Checkpoint Store** holding versioned sparse deltas and collected rollouts. **Rollout Actors** are distributed Rollout Actors spanning heterogeneous hardware across geographic regions (H100, A100, and L40 clusters in the figure); they receive policy deltas, claim prompts, generate rollouts locally, and return results. In each region, one Actor is designated as the **Relay**, a dual-role node that both generates rollouts and serves as a regional proxy. The Relay caches the current policy version v_t and forwards deltas to peer Actors in its region, reducing cross-region traffic from $O(N)$ transfers to one per region. **Workflow.** SparrowRL enforces a strict one-step policy lag [54], bounding staleness while allowing rollouts, update transfer, and version preparation to overlap across regions. In Figure 5, the data plane carries two types of traffic: gray arrows denote rollout traffic and blue arrows denote sparse delta transfer. The control plane handles job coordination

through time-bounded leases: the Job Ledger issues prompts to Actors, and Actors later submit results. Each iteration proceeds through five stages, as annotated in Figure 5. The Job Ledger issues prompts to Actors (1), which generate rollouts on their active version π_v . Completed rollouts flow back (2) to the Checkpoint Store, where they are aggregated for training. The optimizer consumes the collected rollouts and produces the updated policy π_{v+1} (3). The update is encoded as a sparse delta \mathcal{D}_{v+1} , stored in the Checkpoint Store (4), and transferred outward through Relays. Relays forward \mathcal{D}_{v+1} (5) and Actors activate the new version between batches, while laggards catch up asynchronously without blocking other regions. Lease expiry automatically returns orphaned prompts to the pool, avoiding global stalls on stragglers.

5 SYSTEM DESIGN

This section describes four mechanisms within SparrowRL: sparse delta checkpoints (§ 5.1), streaming delta transfer (§ 5.2), heterogeneity-aware scheduling (§ 5.3), and lease-based fault tolerance (§ 5.4).

5.1 Lossless Sparse Delta Geo-Checkpoints

Distributed training frameworks typically decouple parameter persistence from synchronization, saving dense model checkpoints to storage while broadcasting updates over RDMA or NVLink protocols. This separation creates consistency challenges in geo-distributed deployments where network faults are common. If a transfer is interrupted or retried, the system struggles to verify whether a remote Actor has successfully applied the update. Consequently, ensuring that a generated rollout corresponds to a specific training version becomes a complex state-tracking problem rather than a verifiable property.

SparrowRL addresses this by unifying checkpoint storage and network transfer into a single abstraction: the *delta checkpoint*. Rather than sending ephemeral updates, the Trainer produces a versioned, immutable file \mathcal{D}_v for each step, complete with a unique identifier and integrity hash. This design embeds the version control inherent to storage systems directly into the transport layer. By treating network transfer as the replication of a persistent artifact, SparrowRL ensures that partial failures never result in ambiguous states. This unification simplifies the distributed protocol, naturally supporting safe Relay caching, peer-assisted fanout, and verifiable acceptance predicates (§ 5.4).

Sparse encoding. As illustrated in Figure 6, the Trainer flattens each tensor’s delta into a one-dimensional index space and stores the non-zeros as two 1D arrays, idx and val . For attention and MLP projections, SparrowRL writes deltas under fused inference names by stacking split HuggingFace

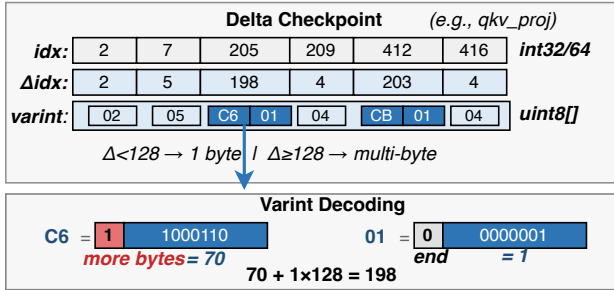


Figure 6: Delta checkpoint index encoding. First, absolute indices (int32/64) are replaced with delta offsets (Δ idx) relative to the previous index. Then, each offset is encoded as a variable-length unsigned byte sequence: offsets < 128 take one byte, while larger offsets use multiple bytes with a high-bit continuation flag.

blocks in a fixed order. For example, Q, K, and V updates become a single *qkv_proj* delta by adding deterministic block offsets to each component’s linear indices. Similarly, Gate and Up matrices fuse into *gate_up_proj*. Actors apply the update with a flat scatter-add over the parameter’s storage, keeping the payload directly consumable by the inference engine.

A naive encoding represents each nonzero update as a fixed-width (index, value) pair, with an int32 or int64 index (depending on tensor size) and a bfloat16 value, thereby dedicating two-thirds or more of the payload to position metadata. SparrowRL reduces this overhead with two complementary techniques. First, it applies *delta encoding* to the sorted index array: the encoder stores the first index as-is, then replaces each subsequent index with its difference from the predecessor. Since non-zero updates are scattered across the tensor, most index differences are small and would fit within an 8-bit unsigned integer. However, rare large gaps make a fixed-width uint8 insufficient. To efficiently capture this long-tailed distribution without over-provisioning every entry, SparrowRL encodes the delta sequence using unsigned LEB128, a variable-length integer representation in which the most significant bit of each byte indicates continuation. Differences smaller than 128 therefore occupy a single byte, while larger gaps extend to multiple bytes. For example, the value 198 is encoded as two bytes (C6 01). The first byte C6 (1100 0110₂) carries payload 70 and sets the continuation bit, indicating that additional bytes follow. The second byte 01 (0000 0001₂) carries payload 1 as the final byte. Interpreting the payload in LEB128 yields $70 + (1 \ll 7) = 198$ (Figure 6). Together, these techniques reduce the index footprint from four bytes per entry to fewer than two on average, further cutting total checkpoint size by 30–50%.

Lossless precision. Unlike gradient compression techniques [27] that trade accuracy for bandwidth through lossy quantization, SparrowRL employs purely lossless compression. The non-zero parameter based delta-encoded varint representation preserves full precision for the values, ensuring that Actors receive exactly the same update as the Trainer.

5.2 Streaming Delta Transfer Protocol

Sparse encoding reduces transfer volume, but transfer must still complete quickly enough to keep Actors within SparrowRL’s one-step lag bound. This creates a per-iteration deadline: each Actor should finish staging \mathcal{D}_{v+1} before it completes its current rollout batch on π_v , otherwise it will either idle waiting for the next version or fall behind and become unable to contribute valid rollouts.

In our US–Canada deployment with Qwen3-8B in § 7, extracting a sparse delta takes approximately 5 s, while transferring a 202 MB delta over a single TCP stream takes 4.71 s. Even after sparsity reduces payload size, the WAN transport is still sensitive to large bandwidth-delay products and loss, and a single stream commonly leaves capacity unused due to congestion control and head-of-line blocking. SparrowRL therefore treats each delta checkpoint as a stream and accelerates transfer with two techniques targeting tail latency.

First, it pipelines extraction with cut-through forwarding, allowing transmission to begin before the full delta is materialized. Second, it stripes segments across multiple parallel TCP streams so that loss-induced stalls on one stream do not block the others, keeping the link busy under transient loss.

Overlapped extraction and transfer. As illustrated in Figure 7, the Trainer extracts the sparse delta by scanning parameters and encoding nonzeros. Instead of treating \mathcal{D}_v as a monolithic file, SparrowRL packetizes it into a sequence of segments that can be transmitted and buffered independently and reassembled deterministically, with integrity verified against the delta checkpoint hash. The Trainer emits each segment immediately after encoding it, and Relays forward segments on arrival, creating cut-through overlap between extraction, cross-region transfer, and intra-region fanout.

SparrowRL uses S parallel TCP streams and stripes segments round-robin across them. Segment-level striping serves two purposes. First, it improves link utilization on WAN paths where a single TCP stream underutilizes bandwidth due to conservative congestion control. Second, it reduces long-tail sensitivity to loss: a retransmission stall on one stream delays only its assigned segments, while other streams continue to make progress. This granularity also avoids imbalance under skewed sparsity patterns where a small subset of layers carries most of the delta bytes. In our deployment, multi-stream reduces per-step transfer time

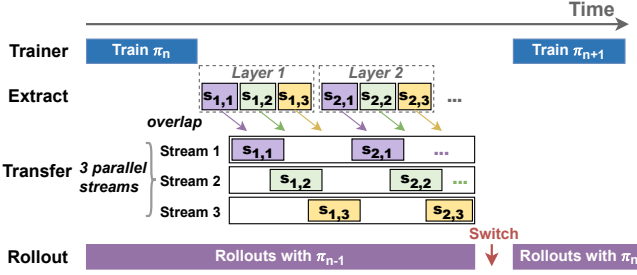


Figure 7: Pipelined delta extraction and multi-stream transfer ($S=3$). Segments are striped round-robin across parallel streams, overlapping extraction with transmission. Actors continue rollouts on π_{n-1} and switch to π_n when transfer completes.

from 4.71 s to 2.90 s without changing payload size. Finally, SparrowRL overlaps transfer with rollout generation: Actors stage \mathcal{D}_{v+1} while generating on π_v , so activation can occur at the next safe point instead of blocking on transfer.

Relay-based fanout. Multi-stream transfer accelerates delivery to a single receiver, but transfer must also scale to many Actors per region without imposing $O(N)$ cross-region transfers. SparrowRL therefore adopts a relay-based, two-tier push transfer path. For each remote region, the Trainer streams \mathcal{D}_v only to a designated seed Actor, which acts as a relay and proactively forwards the staged update to the peer Actors in that region. The relay forwards blocks as they arrive, overlapping cross-region reception with intra-region fanout. SparrowRL separates *staging* from *activation*: once the delta is fully staged, the Job Ledger sends a commit command for version v to the relay, and the relay propagates the same commit to its peers so that all Actors switch to v . To preserve consistency under retries and failures, each delta is tagged with a base version, and an Actor accepts/activates \mathcal{D}_v only if its currently active version matches the declared base, preventing out-of-order application.

Staged activation. SparrowRL decouples delta transfer from model activation using a staged-update protocol. This separation is necessary because pipelining and relay forwarding deliver deltas incrementally, and Actors should never serve rollouts from a partially applied policy. Each Actor receives \mathcal{D}_v asynchronously and reassembles it in a local staging buffer while continuing to generate rollouts using its currently active model version. Upon an explicit *commit* for version v , the Actor waits for a safe point (i.e., the end of the current generation batch) and then applies the staged delta in-place via sparse scatter-add to its resident parameters. The Actor advances its active-version tag only after the scatter-add completes, ensuring that rollouts are served

Algorithm 1: Heterogeneity-Aware Job Scheduling

```

Input: Version  $v$ , batch size  $B$ , per-Actor throughput  $\tau_a$ ,  

exclusion decay factor  $\alpha$ , EMA factor  $\beta$ 
1  $T \leftarrow 0$ ;
2 foreach registered Actor  $a$  do
3   if  $a.ver = v$  or  $a.ver = v-1$  then
4      $| T \leftarrow T + \tau_a$ 
5   end
6 end
7 foreach registered Actor  $a$  do
8   if  $a.ver = v$  or  $a.ver = v-1$  then
9      $| B_a \leftarrow \lfloor B \cdot \tau_a / T \rfloor$ ;
10    if  $a.ver = v-1$  then
11       $| \text{send COMMIT}(v) \text{ to } a$ ;
12    end
13    dispatch  $B_a$  requests to  $a$ ;
14  else  $B_a \leftarrow 0$ ,  $\tau_a \leftarrow \alpha \tau_a$ ;
15 end
16 On settle:  $\tau_a \leftarrow \beta \tau_a + (1-\beta) \cdot (\text{tokens/elapsed})$ ;

```

by a consistent model snapshot and never observe partially applied updates during generation.

5.3 Heterogeneity-Aware Scheduling

Actors vary widely in compute capacity (A100 vs. H100 differs by 2–3×) and network bandwidth, and these gaps shift over time as links congest, GPUs throttle, and spot instances are preempted. Equal work assignment creates stragglers, and because SparrowRL enforces a one-step policy lag, an Actor that falls two steps behind has its rollouts invalidated.

SparrowRL addresses this with two mechanisms. *Adaptive job allocation* splits each batch proportionally to estimated throughput, implicitly penalizing slow Actors via EMA-updated estimates. *Version-aware scheduling* gates participation on each Actor’s version state, ensuring that only Actors capable of running the target policy version receive work. Algorithm 1 summarizes the logic.

Adaptive job allocation. The user specifies a total batch size B per training step, and the Trainer splits B across eligible Actors in proportion to their estimated generation throughput so that all Actors finish at approximately the same time. The Trainer maintains a per-Actor throughput estimate τ_a (tokens/s) and computes the eligible aggregate capacity $T = \sum_{a \in \mathcal{E}} \tau_a$, where \mathcal{E} is the set of Actors whose version state permits participation (line 4). Each eligible Actor a then receives $B_a = \lfloor B \cdot \tau_a / T \rfloor$ requests (line 9). For example, an H100 at 5,000 tokens/s and an A100 at 2,500 tokens/s split a batch of 300 requests into 200 and 100, respectively.

The scheduler adapts to changing conditions automatically. After each settlement, the Trainer updates τ_a via exponential moving average (line 16), blending the historical

estimate with the Actor’s recent throughput. Because B_a is proportional to τ_a/T , a slower Actor sees its τ_a drop and consequently its share of the next batch shrink, while faster Actors receive more requests. This single feedback signal captures all sources of slowdown, including GPU throttling, network congestion that delays delta transfers, and transient resource contention, without requiring separate bandwidth-tracking mechanism.

Version-aware scheduling. Before assigning a new batch, the Trainer checks each Actor’s version state to determine eligibility (line 4). An Actor qualifies if it is already on version v , or if it is on $v-1$ with delta v being staged. Actors on $v-1$ receive a COMMIT for version v (line 11) so they activate the staged delta before generating rollouts. Actors that are more than one version behind are temporarily excluded (line 14) and receive no work for the current step. This decision avoids partial allocation: the entire batch is distributed only among eligible Actors. Exclusion applies a decay α to τ_a , so rejoining Actors start conservatively and recover throughput share only after demonstrating sustained performance.

5.4 Fault Tolerance

In SparrowRL, two fault classes may happen: *actor-side faults* from GPU preemption or process crashes, and *network faults* from cross-region link outages between Trainer and Actors. SparrowRL handles both through lease-based coordination that detects failures implicitly and redistributes work without global barriers. Each Actor holds a time-bounded lease (2–3× median completion time) on its claimed prompts; if it fails to submit before expiry, those prompts automatically return to the pool for reassignment by surviving Actors. Cross-region link failures trigger the same path: partitioned Actors’ leases expire and connected Actors absorb their work. To prevent stale rollouts from poisoning training, the Trainer accepts result r only if the lease remains valid ($t_r \leq t_j^{\text{expire}}$), the behavior version matches ($v_r = v_j$), and the checkpoint hash matches ($h_r = h(v_j)$). When a Relay fails, Actors fetch deltas directly from the Trainer or peers; Trainer failures are handled by standard checkpoint-and-restart.

6 DISCUSSION

Distributed training. Geo-distributed gradient aggregation is well studied [4, 6, 7, 27]. SparrowRL focuses on a distinct challenge in RL: frequent policy transfer to Actors, which dominates cross-region cost due to RL’s asymmetric pipeline. Combining SparrowRL with distributed training techniques is promising future work.

Positioning. SparrowRL can serve a dual purpose across different scales of operation. For academia and smaller organizations, it provides an economic alternative to dedicated clusters, improving cost efficiency by unlocking cheaper,

loosely connected GPU pools that would otherwise be unusable for RL training. For large-scale industrial scenarios, SparrowRL addresses the network bottlenecks inherent in disaggregated architectures. By bridging these network challenges, it enables the real use of heterogeneous hardware within a single cloud, dedicating high-bandwidth GPUs for training while employing cost-effective inference accelerators for rollout generation.

7 EXPERIMENT

We build SparrowRL (~4.3K lines of Python codes) atop the PrimeRL framework with PyTorch FSDP2 [39] and vLLM [25] as underlying training and inference engines.

7.1 Experimental Setup

Testbed. We evaluate SparrowRL across geo-distributed GPU deployments spanning multiple continents. All machines run Ubuntu 24.04.1 with CUDA 12.6. The Trainer uses FSDP2 for distributed optimization, while Rollout Actors use vLLM for inference. We evaluate Qwen3 models [49] at 4B, 8B, and 14B, using 2/4/6×H100 (SXM5) GPUs for training and 4/8/12 Actors, each deployed on a single A100 (PCIe) GPU. The Trainer is deployed in the U.S., while Actors run in Canada, connected by a commodity cross-cloud WAN link whose measured bandwidth fluctuates between 500 Mbps and 1 Gbps, exhibiting substantial temporal and cross-provider variability commonly observed in cross-cloud connectivity. Unless otherwise stated, all experiments use this native cross-cloud WAN link. Additionally, to characterize the robustness of SparrowRL, we vary (i) network bandwidth via controlled emulation from 0.25 to 10 Gbps using Linux traffic control (tc) [22] (§ 7.4), (ii) geographic distribution by placing inference Actors across datacenters in Japan, the Netherlands, Iceland, and Australia (§ 7.5), and (iii) inference heterogeneity by mixing A100 and L40 GPUs across Actors (§ 7.6).

Models and datasets. We evaluate SparrowRL using the widely-adopted GRPO algorithm [41] on three reasoning benchmarks: Hendrycks MATH [46], GSM8K [8], and DeepScaleR [31]. We use the Qwen3 model family [49] with 4B, 8B, and 14B parameters. For each run, the Trainer dispatches rollout jobs requiring each Actor to generate a rollout group of size $G = 512$. Each experiment executes seven optimizer steps with a fixed one-step asynchronous policy.

Baselines. We compare SparrowRL against three baselines. *Ideal-SingleDC* is an idealized baseline that collocates the Trainer and all Actors within a single datacenter connected by high-bandwidth RDMA (800 Gbps) and NVLink (900 GB/s). We construct this baseline by replacing the cross-cloud weight transfer cost in SparrowRL’s measured execution traces with the corresponding RDMA transfer cost,

keeping other components unchanged. This yields an idealized upper bound for the RL system. *PrimeRL-Full* ports PrimeRL [21] to a geo-distributed setting by broadcasting the full model parameters after every optimizer step, exposing the cost of full-weight synchronization over WAN links. *PrimeRL-MultiStream* further improves bandwidth utilization by transferring full model weights over multiple network streams. Across all systems, we keep the Trainer implementation, Actor count, and configuration identical.

Metrics. We report two primary metrics following prior work on RL training systems [54, 55]. *Training step time* measures the wall-clock duration of a single optimizer step, including weight synchronization, rollout generation, and gradient computation. *Throughput* captures the average number of tokens processed per second across the entire system.

7.2 End-to-End Results

We first evaluate end-to-end RL training performance under real-world geo-distributed conditions.

Throughput. Figure 8(a) reports end-to-end throughput across all benchmarks and model sizes. SparrowRL consistently outperforms PrimeRL-Full and PrimeRL-MultiStream, while closely approaching Ideal-SingleDC. As model size increases, the performance gap between SparrowRL and full weight transfer baselines widens. On Qwen3-4B, SparrowRL improves throughput by $2.4\times$ – $3.7\times$ over PrimeRL-Full; on Qwen3-14B, the improvement grows to $7.7\times$ – $9.5\times$ across all benchmarks. Under PrimeRL-Full, throughput degrades rapidly with model scale because the communication of full model parameters is now the critical path. PrimeRL-MultiStream improves bandwidth utilization by transferring chunked dense weights over multiple parallel TCP streams, yielding up to $2.1\times$ higher throughput than PrimeRL-Full. However, synchronization remains blocking and continues to dominate the step time for larger models, leaving a $1.5\times$ – $6.0\times$ throughput gap relative to SparrowRL. In contrast, SparrowRL keeps weight transfer off the critical path, so end-to-end performance is governed by rollout generation and training computation rather than parameter transfer.

Step time. Figure 8(b) shows the average step time. Under PrimeRL-Full, step time increases sharply with model size, exceeding 500 seconds for Qwen3-14B. Although a one-step policy lag allows Actors to continue generating rollouts using the previous policy, dense model weights must still be delivered before each new policy version can be activated. Over WAN links, this delivery cost substantially slows down overall training progress. PrimeRL-MultiStream improves bandwidth utilization, but dense weight transfer remains on the critical path and therefore continues to dominate step time. In contrast, SparrowRL consistently achieves step times close to Ideal-SingleDC by combining sparse delta updates

(reducing transfer volume, § 5.1) with the streaming delta transfer protocol (§ 5.2), which together hide synchronization latency from the critical path.

Gap to ideal performance. Compared to Ideal-SingleDC, SparrowRL is within 1.31%–8.91% of the single-DC throughput across all configurations. The small remaining gap stems from two sources: (1) residual WAN latency for delta delivery and control-plane messages, and (2) CPU-side delta extraction overhead per step, neither of which exists on an RDMA fabric. Both costs are largely hidden by overlap with rollout generation but cannot be fully eliminated. Despite these residual overheads, SparrowRL narrows the throughput gap from 59.0%–90.3% under PrimeRL-Full (37.3%–84.5% under PrimeRL-MultiStream) to within 1.31%–8.91%, demonstrating that sparse transfer enables practical wide-area RL training without sacrificing efficiency.

7.3 Ablation Study

We isolate each mechanism’s contribution using Qwen3-8B with the same configuration as § 7.2.

Execution timeline. A primary goal of SparrowRL is to reduce the cost of weight synchronization on step time. We therefore compare PrimeRL-Full and SparrowRL in terms of update size, transfer time, and overlap with rollout generation. Figure 9 shows the execution timeline for five consecutive training steps when training Qwen3-8B. Under PrimeRL-Full, each step broadcasts the full model weights, leading to transfer times of around 200 s for each step. Although Actors use a one-step policy lag, dense weight transfer still appears as a per-step overhead. As a result, completing five steps takes 15 min 48 s, with synchronization dominating step execution. In contrast, SparrowRL completes five steps in 5 min 9 s. Sparse deltas reduce the per-step payload from 15.6 GB to 202 MB, and delta extraction and transfer (7–12 s per step) overlap with rollout generation, contributing little to overall step time.

Encoding optimization. Figure 10 reports per-step delta transfer cost for Qwen3-8B over the US–Canada WAN link. Compared to a naive `int32/64` index encoding, the `uint8` delta encoding (Figure 6) reduces the per-step payload from 414 MB to 202 MB, cutting transfer time from 9.22 s to 4.71 s. Even with compact deltas, a single TCP stream underutilizes the link; enabling multi-stream transfer further reduces transfer time to 2.90 s.

Streaming optimization. We evaluate whether transport-level parallelism further improves performance once sparse deltas are applied. As shown in Figure 11, using four parallel TCP streams improves throughput by 8.2% on GSM8K and 11.7% on DeepScaleR for Qwen3-8B, and by 12.4% on GSM8K and 16.3% on DeepScaleR for Qwen3-14B. Larger

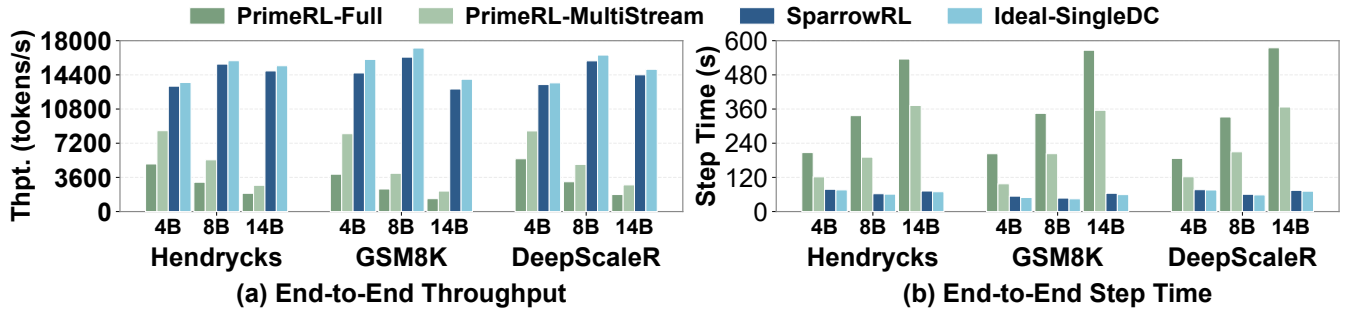


Figure 8: End-to-end (a) throughput and (b) step time under geo-distributed deployment across three benchmarks and Qwen3 model sizes. SparrowRL approaches Ideal-SingleDC and outperforms PrimeRL-Full.

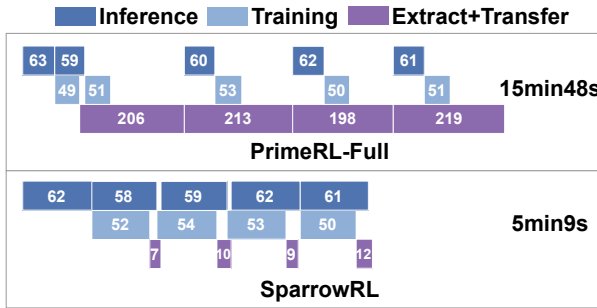


Figure 9: Workflow timeline: preparation overlaps rollout generation; activation triggers a version switch; laggards catch up asynchronously.

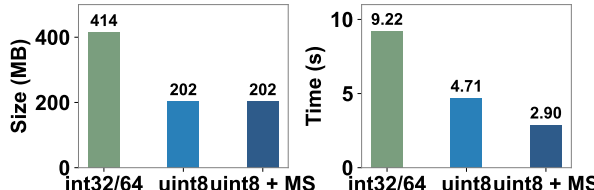


Figure 10: Per-step delta transfer cost for Qwen3-8B (US-Canada). MS denotes multi-stream transport.

models benefit more because they produce larger delta payloads, making transfer a bigger fraction of the step time and increasing the payoff of better bandwidth utilization. These gains indicate that transport parallelism improves bandwidth utilization and reduces the communication time, yielding moderate throughput gains in the end-to-end pipeline, where training and rollout generation dominate the step time.

Relay optimization. When multiple Actors share a remote region, SparrowRL supports Relay-based distribution: the Trainer sends each delta once to a Relay node that forwards locally, reducing cross-region bandwidth at the cost of a

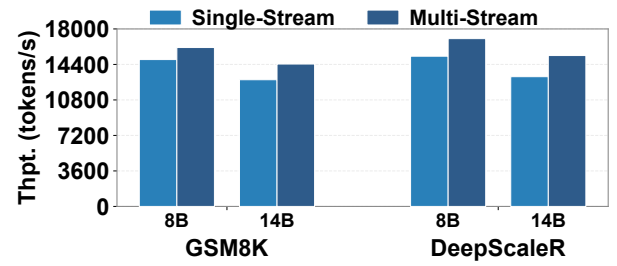


Figure 11: Throughput with single-stream versus multi-stream delta transfer across two datasets.

Table 5: End-to-end throughput with and without relay-based delta distribution.

Dataset	Baseline	Relay	Improvement
GSM8K	13558.4	14188.1	+4.4%
DeepScaleR	14060.0	16012.7	+13.9%

small additional hop. Table 5 compares end-to-end throughput with and without Relays under a Canada–Australia deployment. Using a Relay consistently improves throughput across both benchmarks, with a larger gain on DeepScaleR. These results show that Relay-based distribution is beneficial when Rollout Actors share a common WAN ingress. While the absolute improvement is modest for Qwen3-8B, the benefit of Relays is expected to grow with model size, as larger models incur higher cross-region delta transfer costs.

7.4 Sensitivity to Network Bandwidth

Bandwidth is the primary constraint in geo-distributed deployments and can vary widely across providers and regions. We therefore evaluate how transfer cost changes as available bandwidth decreases, by emulating links from 250 Mbps to 10 Gbps using Linux traffic control (tc) [22]. In Figure 12, PrimeRL-Full (*Full*) must broadcast dense weights every step,

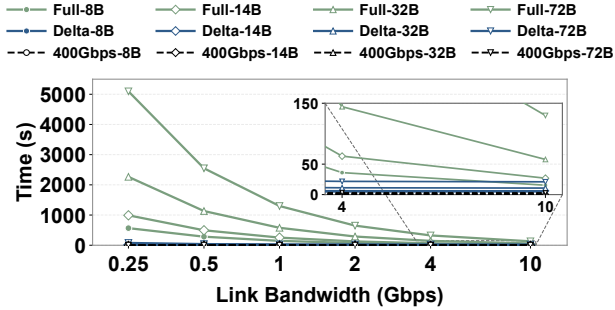


Figure 12: Per-step weight transfer time under emulated bandwidth constraints.

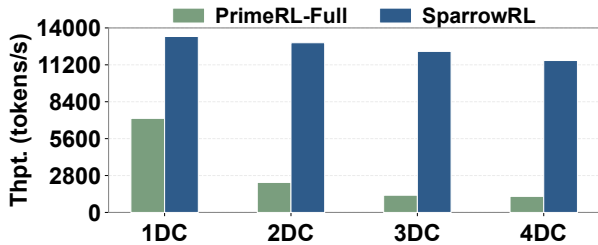


Figure 13: End-to-end throughput as Actors span 1–4 geographically distributed data centers (DCs) (Qwen3-4B, 2×H100 Trainer, 4×A100 Actors).

while SparrowRL (*Delta*) transfers sparse deltas. PrimeRL-Full transfer time scales inversely with bandwidth, rising from 17.3 s at 10 Gbps to 566 s at 250 Mbps for the 8B model, and growing further with model size. In contrast, SparrowRL is far less sensitive to bandwidth and stays sub-second at 10 Gbps. For example, at 10 Gbps, SparrowRL transfers deltas for Qwen3-8B in 0.32 s, which closely matches the 0.32 s required to broadcast full weights over an ideal 400 Gbps RDMA fabric. This trend holds across model scales, indicating that sparsity-aware delta transfer can compensate for orders of magnitude lower bandwidth.

7.5 Multi-Datacenter Results

Beyond the two-DC setup above, SparrowRL can also leverage available GPUs across multiple geographic regions as inference Actors. We evaluate how SparrowRL scales when inference Actors are spread across multiple datacenters. The Trainer runs Qwen3-4B on 2×H100 GPUs in the US, while four A100 inference Actors are placed across one to four regions: Canada only (1-DC), Canada and Japan (2-DC), Canada, Japan, and the Netherlands (3-DC), and Canada, Japan, the Netherlands, and Iceland (4-DC). As shown in Figure 13, PrimeRL-Full throughput drops sharply as more datacenters are added, from 7,137 tokens/s in a single region

to 1,219 tokens/s across four regions, a 5.86× reduction. This drop occurs because PrimeRL-Full’s transfer is bounded by the slowest Actor, and adding distant datacenters increases tail latency. In contrast, SparrowRL maintains much more stable throughput, decreasing by only 13.7% from one to four regions. Compared to PrimeRL-Full, SparrowRL achieves 1.9×–9× higher throughput as geographic dispersion increases. These results indicate that sparse delta transfer scales better than full weight transfer as Actors span multiple datacenters.

7.6 Heterogeneous GPU Results

Moreover, real-world geo-distributed inference pools are rarely homogeneous: GPU types and connection links vary across regions and providers. Such heterogeneity exacerbates straggler effects, making uniform rollout assignment inefficient and underutilizing faster Actors. We evaluate heterogeneity-aware load balancing by training Qwen3-4B on 4×H100 GPUs in Canada, with inference served by a heterogeneous pool of 4×A100 and 4×L40 GPUs in the US. As shown in Table 7, dynamically assigning requests based on observed Actor throughput improves end-to-end performance by 26.4%–35.5% over uniform distribution. These results demonstrate that heterogeneity-aware scheduling is essential for efficiently utilizing diverse and imbalanced inference Actors in geo-distributed RL training.

7.7 Cost-Effectiveness Analysis

Ultimately, the goal of SparrowRL is to make RL training economically viable using on-demand, cross-cloud capacity. We evaluate cost efficiency using throughput per dollar (tokens/\$). To ensure a fair comparison, we derive the cost of the Ideal Single-DC baseline and SparrowRL from representative deployment options as shown in Table 6.

We use these hourly prices when computing tokens/\$. Reserved RDMA clusters are typically homogeneous and provisioned in fixed 8-GPU blocks, so the Ideal Single-DC baseline uses H100-only RDMA clusters and does not mix GPU types across training and inference. For our inference Actors, one H100 delivers throughput comparable to two A100s, so 4H100 + 8A100 is roughly capacity-matched to 1×8×H100, while 6H100 + 12A100 corresponds to roughly 12 H100s and must round up to 2×8×H100. RDMA clusters also impose minimum commitments (24 hours to one week), but we compute tokens/\$ using the amortized \$/hr rates, which assumes full utilization of the minimum commitment and therefore favors SingleDC for short RL post-training runs. Table 6 reports cost efficiency using the geometric mean throughput across all benchmarks. Across model sizes, SparrowRL achieves throughput comparable to the Single-DC baseline while incurring lower hourly cost. As shown in Table 6, SparrowRL improves tokens/\$ by 1.21× for Qwen3-8B

Table 6: Cost efficiency of SparrowRL compared to Ideal-SingleDC. Cross-cloud deployments use on-demand H100s from Hyperbolic [19] and A100s from Prime Intellect [38] with standard VM networking; SingleDC uses reserved RDMA clusters from Hyperbolic. Throughput is the geometric mean across Hendrycks MATH, GSM8K, and DeepScaleR. Data egress fees are omitted as they are negligible compared to GPU cost.

Model	Method	Configuration	BW	GM Throughput (tokens/s)	\$/hr	tokens/\$ ($\times 10^6$)	Norm. (SingleDC=1)
Qwen3-8B	SparrowRL	4xH100 + 8xA100 (cross-cloud on-demand)	~1 Gbps	~15.9k	15.88	~3.60	1.21x
	SingleDC	1x8xH100 RDMA cluster (reserved)	≥ 800 Gbps	~16.5k	19.92	~2.99	1.0x
Qwen3-14B	SparrowRL	6xH100 + 12xA100 (cross-cloud on-demand)	~1 Gbps	~14.0k	23.82	~2.12	1.59x
	SingleDC	2x8xH100 RDMA cluster (reserved)	≥ 800 Gbps	~14.8k	39.84	~1.33	1.0x

Table 7: End-to-end throughput (tokens/s) under heterogeneous inference deployment (A100 + L40) with uniform versus heterogeneity-aware load balancing.

Dataset	Uniform	Heterogeneity-aware	Improvement
GSM8K	10414.6	14107.6	+35.5%
DeepScaleR	10755.1	13589.9	+26.4%

and 1.59x for Qwen3-14B. These results indicate that, even when compared against an idealized Single-DC deployment with full RDMA connectivity, WAN-aware disaggregation can yield measurable cost-efficiency gains under real cross-cloud pricing.

8 RELATED WORK

RL Systems in a Single Datacenter. As discussed in § 2.3, state-of-the-art RL systems such as OpenRLHF [18], veRL [43], and StreamRL [54] optimize throughput through hybrid execution and disaggregated architectures, while rollout accelerators including RhymeRL [16], APRIL [56], Sorte-dRL [53], RollPacker [12], and RLHFuse [55] reduce generation latency. OPPO [48] further improves efficiency by overlapping generation with scoring through token streaming and by deferring long-tail sequences across steps. These techniques assume high-bandwidth intra-datacenter networks and primarily address intra-cluster inefficiencies. SparrowRL complements these approaches: it can integrate the above works to maximize intra-region efficiency while addressing the orthogonal challenge of inter-region weight transfer.

Cross-datacenter training. Geo-distributed training systems address bandwidth constraints for *training-time* communication. MAST [7] schedules jobs across regions to reduce transfers; Varuna [4] and CrossPipe [6] use pipeline parallelism and network-aware scheduling; StellaTrain [27] combines compression with bounded staleness; Ooblec [23] and Bagpipe [1] improve robustness and overlap communication with compute. However, these approaches optimize gradients and intermediate tensors among training workers,

whereas cross-region RL faces a different critical path: frequent policy synchronization from a (typically) centralized optimizer to geographically dispersed rollout workers.

9 CONCLUSION

SparrowRL is a novel system to enable practical RL post-training of LLMs over geo-distributed GPUs without hurting model accuracy. By co-designing system mechanisms with the inherent sparsity of RL weight updates, SparrowRL closes the performance gap between commodity WAN links and tightly coupled RDMA clusters, broadening access to frontier model training for researchers and organizations worldwide.

REFERENCES

- [1] Saurabh Agarwal, Chengpo Yan, Ziyi Zhang, and Shivaram Venkataraman. 2023. Bagpipe: Accelerating Deep Recommendation Model Training. In *Proceedings of the 29th Symposium on Operating Systems Principles (SOSP '23)*. Association for Computing Machinery, New York, NY, USA, 348–363. <https://doi.org/10.1145/3600006.3613142>
- [2] Arash Ahmadian, Chris Cremer, Matthias Gallé, Marzieh Fadaee, Julia Kreutzer, Olivier Pietquin, Ahmet Üstün, and Sara Hooker. 2024. Back to Basics: Revisiting REINFORCE Style Optimization for Learning from Human Feedback in LLMs. (2024). arXiv:cs.LG/2402.14740 <https://arxiv.org/abs/2402.14740>
- [3] Amazon Web Services. 2026. AWS EC2 Price Calculator. <https://calculator.aws/#/createCalculator/ec2-enhancement>. (2026). Accessed: 2026-01.
- [4] Sanjith Athlur, Nitika Saran, Muthian Sivathanu, Ramachandran Ramjee, and Nipun Kwatra. 2022. Varuna: scalable, low-cost training of massive deep learning models. In *Proceedings of the Seventeenth European Conference on Computer Systems (EuroSys '22)*. Association for Computing Machinery, New York, NY, USA, 472–487. <https://doi.org/10.1145/3492321.3519584>
- [5] Alexander Borzunov, Dmitry Baranchuk, Tim Dettmers, Max Ryabinin, Younes Belkada, Artem Chumachenko, Pavel Samygin, and Colin Raffel. 2023. Petals: Collaborative Inference and Fine-tuning of Large Models. (2023). arXiv:cs.LG/2209.01188 <https://arxiv.org/abs/2209.01188>
- [6] Tiancheng Chen, Ales Kubicek, Langwen Huang, and Torsten Hoefer. 2025. CrossPipe: towards optimal pipeline schedules for cross-datacenter training. In *Proceedings of the 2025 USENIX Conference on Usenix Annual Technical Conference (USENIX ATC '25)*. USENIX Association, USA, Article 64, 20 pages.
- [7] Arnab Choudhury, Yang Wang, Tuomas Pelkonen, Kutta Srinivasan, Abha Jain, Shenghao Lin, Delia David, Siavash Soleimanifard, Michael

Chen, Abhishek Yadav, Ritesh Tijoriwala, Denis Samoylov, and Chun-
qiang Tang. 2024. MAST: global scheduling of ML training across
geo-distributed datacenters at hyperscale. In *Proceedings of the 18th
USENIX Conference on Operating Systems Design and Implementation
(OSDI'24)*. USENIX Association, USA, Article 30, 18 pages.

[8] Karl Cobbe, Vineet Kosaraju, Mohammad Bavarian, Mark Chen, Heewoo Jun, Lukasz Kaiser, Matthias Plappert, Jerry Tworek, Jacob Hilton, Reiichiro Nakano, Christopher Hesse, and John Schulman. 2021. Training Verifiers to Solve Math Word Problems. (2021). arXiv:cs.LG/2110.14168 <https://arxiv.org/abs/2110.14168>

[9] Abhimanyu Dubey, Abhinav Jauhri, Abhinav Pandey, Abhishek Kadian, Ahmad Al-Dahle, Aiesha Letman, Akhil Mathur, Alan Schelten, Amy Yang, Angela Fan, et al. 2024. The llama 3 herd of models. *arXiv e-prints* (2024), arXiv-2407.

[10] Alexander Erben, Ruben Mayer, and Hans-Arno Jacobsen. 2024. How Can We Train Deep Learning Models Across Clouds and Continents? An Experimental Study. *Proc. VLDB Endow.* 17, 6 (Feb. 2024), 1214–1226. <https://doi.org/10.14778/3648160.3648165>

[11] Wei Fu, Jiaxuan Gao, Xujie Shen, Chen Zhu, Zhiyu Mei, Chuiy He, Shusheng Xu, Guo Wei, Jun Mei, Jiashu Wang, Tongkai Yang, Binhang Yuan, and Yi Wu. 2025. AReAL: A Large-Scale Asynchronous Reinforcement Learning System for Language Reasoning. (2025). arXiv:cs.LG/2505.24298 <https://arxiv.org/abs/2505.24298>

[12] Wei Gao, Yuheng Zhao, Dakai An, Tianyuan Wu, Lunxi Cao, Shaopan Xiong, Ju Huang, Weixun Wang, Siran Yang, Wenbo Su, Jiamang Wang, Lin Qu, Bo Zheng, and Wei Wang. 2025. RollPacker: Mitigating Long-Tail Rollouts for Fast, Synchronous RL Post-Training. (2025). arXiv:cs.DC/2509.21009 <https://arxiv.org/abs/2509.21009>

[13] Google Cloud. 2025. Google Cloud Pricing Calculator. <https://cloud.google.com/products/calculator>. (2025). Accessed: 2026-01.

[14] Daya Guo, Dejian Yang, Haowei Zhang, Junxiao Song, Ruoyu Zhang, Runxin Xu, Qihao Zhu, Shirong Ma, Peiyi Wang, Xiao Bi, et al. 2025. Deepseek-r1: Incentivizing reasoning capability in llms via reinforcement learning. *arXiv preprint arXiv:2501.12948* (2025).

[15] Yaru Hao, Li Dong, Xun Wu, Shaohan Huang, Zewen Chi, and Furu Wei. 2025. On-Policy RL with Optimal Reward Baseline. (2025). arXiv:cs.LG/2505.23585 <https://arxiv.org/abs/2505.23585>

[16] Jingkai He, Tianjian Li, Erhu Feng, Dong Du, Qian Liu, Tao Liu, Yubin Xia, and Haibo Chen. 2025. History Rhymes: Accelerating LLM Reinforcement Learning with RhymeRL. (2025). arXiv:cs.LG/2508.18588 <https://arxiv.org/abs/2508.18588>

[17] Yongjun He, Shuai Zhang, Jiading Gai, Xiyuan Zhang, Boran Han, Bernie Wang, Huzefa Rangwala, and George Karypis. 2025. HetRL: Efficient Reinforcement Learning for LLMs in Heterogeneous Environments. (2025). arXiv:cs.DC/2512.12476 <https://arxiv.org/abs/2512.12476>

[18] Jian Hu, Xibin Wu, Wei Shen, Jason Klein Liu, Zilin Zhu, Weixun Wang, Songlin Jiang, Haoran Wang, Hao Chen, Bin Chen, Weikai Fang, Xianyu, Yu Cao, Haotian Xu, and Yiming Liu. 2025. OpenRLHF: An Easy-to-use, Scalable and High-performance RLHF Framework. (2025). arXiv:cs.AI/2405.11143 <https://arxiv.org/abs/2405.11143>

[19] Hyperbolic AI. 2025. Hyperbolic – The Open-Access AI Cloud. <https://www.hyperbolic.ai>. (2025). Accessed: January 13, 2026.

[20] Hyperstack. 2025. Hyperstack AI Cloud. <https://www.hyperstack.cloud>. (2025). Accessed: January 29, 2026.

[21] Prime Intellect. 2025. PRIME-RL. (2025). <https://github.com/PrimeIntellect-ai/prime-rl>

[22] iproute2 Project. [n. d.]. Linux Traffic Control (tc). <https://man7.org/linux/man-pages/man8/tc.8.html>. ([n. d.]). Accessed: January 31, 2026.

[23] Insu Jang, Zhenning Yang, Zhen Zhang, Xin Jin, and Mosharaf Chowdhury. 2023. Oobleck: Resilient Distributed Training of Large Models Using Pipeline Templates. In *Proceedings of the 29th Symposium on Operating Systems Principles (SOSP '23)*. Association for Computing Machinery, New York, NY, USA, 382–395. <https://doi.org/10.1145/360006.3613152>

[24] Bowen Jin, Hansi Zeng, Zhenrui Yue, Jinsung Yoon, Sercan Arik, Dong Wang, Hamed Zamani, and Jiawei Han. 2025. Search-R1: Training LLMs to Reason and Leverage Search Engines with Reinforcement Learning. (2025). arXiv:cs.CL/2503.09516 <https://arxiv.org/abs/2503.09516>

[25] Woosuk Kwon, Zhuohan Li, Siyuan Zhuang, Ying Sheng, Lianmin Zheng, Cody Hao Yu, Joseph Gonzalez, Hao Zhang, and Ion Stoica. 2023. Efficient Memory Management for Large Language Model Serving with PagedAttention. In *Proceedings of the 29th Symposium on Operating Systems Principles (SOSP '23)*. Association for Computing Machinery, New York, NY, USA, 611–626. <https://doi.org/10.1145/360006.3613165>

[26] Lambda Cloud. 2026. Running One-Click Clusters. (2026). <https://cloud.lambda.ai/one-click-clusters/running> Accessed: 2026-01-08.

[27] Hwijoon Lim, Juncheol Ye, Sangeetha Abdu Jyothi, and Dongsu Han. 2024. Accelerating Model Training in Multi-cluster Environments with Consumer-grade GPUs. In *Proceedings of the ACM SIGCOMM 2024 Conference (ACM SIGCOMM '24)*. Association for Computing Machinery, New York, NY, USA, 707–720. <https://doi.org/10.1145/3651890.3672228>

[28] Aixin Liu, Bei Feng, Bing Xue, Bingxuan Wang, Bochao Wu, Chengda Lu, Chenggang Zhao, Chengqi Deng, Chenyu Zhang, Chong Ruan, et al. 2024. Deepseek-v3 technical report. *arXiv preprint arXiv:2412.19437* (2024).

[29] Yirui Liu, Lidong Jiang, Deguo Li, Daxiang Kang, ZhaoYang Wei, Yuqi Chai, Bin Niu, Ke Lin, Xiaoning Ding, Jianwen Pi, and Hao Luo. 2025. ByteDance Jakiro: Enabling RDMA and TCP over Virtual Private Cloud. In *Proceedings of the ACM SIGCOMM 2025 Conference (SIGCOMM '25)*. Association for Computing Machinery, New York, NY, USA, 114–128. <https://doi.org/10.1145/3718958.3750496>

[30] Zichen Liu, Changyu Chen, Wenjun Li, Penghui Qi, Tianyu Pang, Chao Du, Wee Sun Lee, and Min Lin. 2025. Understanding R1-Zero-Like Training: A Critical Perspective. (2025). arXiv:cs.LG/2503.20783 <https://arxiv.org/abs/2503.20783>

[31] Michael Luo, Sijun Tan, Justin Wong, Xiaoxiang Shi, William Tang, Manan Roongta, Colin Cai, Jeffrey Luo, Tianjun Zhang, Erran Li, Raluca Ada Popa, and Ion Stoica. 2025. DeepScaleR: Surpassing O1-Preview with a 1.5B Model by Scaling RL. <https://pretty-radio-b75.netotion.site/DeepScaleR-Surpassing-O1-Preview-with-a-1-5B-Model-by-Scaling-RL-19681902c1468005bed8ca303013a4e2>. (2025). Notion Blog.

[32] Matt Ma. 2026. CloudPing - AWS Latency Monitoring. <https://www.cloudping.co/>. (2026). Accessed: 2026-02-03.

[33] Sagnik Mukherjee, Lifan Yuan, Dilek Hakkani-Tur, and Hao Peng. 2025. Reinforcement Learning Finetunes Small Subnetworks in Large Language Models. (2025). arXiv:cs.LG/2505.11711 <https://arxiv.org/abs/2505.11711>

[34] Reiichiro Nakano, Jacob Hilton, Suchir Balaji, Jeff Wu, Long Ouyang, Christina Kim, Christopher Hesse, Shantanu Jain, Vineet Kosaraju, William Saunders, Xu Jiang, Karl Cobbe, Tyna Eloundou, Gretchen Krueger, Kevin Button, Matthew Knight, Benjamin Chess, and John Schulman. 2022. WebGPT: Browser-assisted question-answering with human feedback. (2022). arXiv:cs.CL/2112.09332 <https://arxiv.org/abs/2112.09332>

[35] Michael Noukhovitch, Shengyi Huang, Sophie Xhonneux, Arian Hosseini, Rishabh Agarwal, and Aaron Courville. 2025. Asynchronous RLHF: Faster and More Efficient Off-Policy RL for Language Models. (2025). arXiv:cs.LG/2410.18252 <https://arxiv.org/abs/2410.18252>

[36] OpenAI. 2025. GPT-4o Model | OpenAI API. <https://platform.openai.com/docs/models/gpt-4o>. (2025). Accessed: 2025-12-29.

[37] Perplexity Research. 2025. Weight Transfer for RL Post-Training in under 2 seconds. <https://research.perplexity.ai/articles/weight-transfer-for-rl-post-training-in-under-2-seconds>. (Sept. 2025). Published: 2025-09-24. Accessed: 2026-01-31.

[38] Prime Intellect. 2025. Prime Intellect AI Cloud. <https://www.primeintellect.ai/>. (2025). Accessed: January 31, 2026.

[39] PyTorch. 2025. Getting Started with Fully Sharded Data Parallel (FSDP2). https://docs.pytorch.org/tutorials/intermediate/FSDP_tutorial.html. (2025). Accessed: 2026-01.

[40] Max Ryabinin and Anton Gusev. 2020. Towards Crowdsourced Training of Large Neural Networks using Decentralized Mixture-of-Experts. (2020). arXiv:cs.DC/2002.04013 <https://arxiv.org/abs/2002.04013>

[41] Zhihong Shao, Peiyi Wang, Qihao Zhu, Runxin Xu, Junxiao Song, Xiao Bi, Haowei Zhang, Mingchuan Zhang, Y. K. Li, Y. Wu, and Daya Guo. 2024. DeepSeekMath: Pushing the Limits of Mathematical Reasoning in Open Language Models. (2024). arXiv:cs.CL/2402.03300 <https://arxiv.org/abs/2402.03300>

[42] Idan Shenfeld, Jyothish Pari, and Pukit Agrawal. 2025. RL’s Razor: Why Online Reinforcement Learning Forgets Less. (2025). arXiv:cs.LG/2509.04259 <https://arxiv.org/abs/2509.04259>

[43] Guangming Sheng, Chi Zhang, Zilingfeng Ye, Xibin Wu, Wang Zhang, Ru Zhang, Yanghua Peng, Haibin Lin, and Chuan Wu. 2025. Hybrid-Flow: A Flexible and Efficient RLHF Framework. In *Proceedings of the Twentieth European Conference on Computer Systems (EuroSys ’25)*. Association for Computing Machinery, New York, NY, USA, 1279–1297. <https://doi.org/10.1145/3689031.3696075>

[44] Nisan Stiennon, Long Ouyang, Jeff Wu, Daniel M. Ziegler, Ryan Lowe, Chelsea Voss, Alec Radford, Dario Amodei, and Paul Christiano. 2020. Learning to summarize from human feedback. In *Proceedings of the 34th International Conference on Neural Information Processing Systems (NIPS ’20)*. Curran Associates Inc., Red Hook, NY, USA, Article 253, 14 pages.

[45] Prime Intellect Team, Sami Jaghouar, Justus Mattern, Jack Min Ong, Jannik Straube, Manveer Basra, Aaron Pazdera, Kushal Thaman, Matthew Di Ferrante, Felix Gabriel, Fares Obeid, Kemal Erdem, Michael Keiblinger, and Johannes Hagemann. 2025. INTELLECT-2: A Reasoning Model Trained Through Globally Decentralized Reinforcement Learning. (2025). arXiv:cs.LG/2505.07291 <https://arxiv.org/abs/2505.07291>

[46] Ke Wang, Junting Pan, Weikang Shi, Zimu Lu, Houxing Ren, Aojun Zhou, Mingjie Zhan, and Hongsheng Li. 2024. Measuring multimodal mathematical reasoning with the MATH-vision dataset. In *Proceedings of the 38th International Conference on Neural Information Processing Systems (NIPS ’24)*. Curran Associates Inc., Red Hook, NY, USA, Article 3014, 75 pages.

[47] Qizhen Weng, Wencong Xiao, Yinghao Yu, Wei Wang, Cheng Wang, Jian He, Yong Li, Liping Zhang, Wei Lin, and Yu Ding. 2022. MLaaS in the Wild: Workload Analysis and Scheduling in Large-Scale Heterogeneous GPU Clusters. In *19th USENIX Symposium on Networked Systems Design and Implementation (NSDI 22)*. USENIX Association, Renton, WA, 945–960. <https://www.usenix.org/conference/nsdi22/presentation/weng>

[48] Kaizhuo Yan, Yingjie Yu, Yifan Yu, Haizhong Zheng, and Fan Lai. 2025. OPPO: Accelerating PPO-based RLHF via Pipeline Overlap. (2025). arXiv:cs.LG/2509.25762 <https://arxiv.org/abs/2509.25762>

[49] An Yang, Anfeng Li, Baosong Yang, Beichen Zhang, Binyuan Hui, Bo Zheng, Bowen Yu, Chang Gao, Chengen Huang, Chenxu Lv, et al. 2025. Qwen3 technical report. *arXiv preprint arXiv:2505.09388* (2025).

[50] An Yang, Beichen Zhang, Binyuan Hui, Bofei Gao, Bowen Yu, Chengpeng Li, Dayiheng Liu, Jianhong Tu, Jingren Zhou, Junyang Lin, et al. 2024. Qwen2. 5-math technical report: Toward mathematical expert model via self-improvement. *arXiv preprint arXiv:2409.12122* (2024).

[51] Zongheng Yang, Zhanghao Wu, Michael Luo, Wei-Lin Chiang, Romil Bhardwaj, Woosuk Kwon, Siyuan Zhuang, Frank Sifei Luan, Gautam Mittal, Scott Shenker, and Ion Stoica. 2023. SkyPilot: An Intercloud Broker for Sky Computing. In *20th USENIX Symposium on Networked Systems Design and Implementation (NSDI 23)*. USENIX Association, Boston, MA, 437–455. <https://www.usenix.org/conference/nsdi23/presentation/yang-zongheng>

[52] Jingzhao Zhang, Tianxing He, Suvrit Sra, and Ali Jadbabaie. 2020. Why gradient clipping accelerates training: A theoretical justification for adaptivity. (2020). arXiv:math.OC/1905.11881 <https://arxiv.org/abs/1905.11881>

[53] Yiqi Zhang, Huiqiang Jiang, Xufang Luo, Zhihe Yang, Chengruidong Zhang, Yifei Shen, Dongsheng Li, Yuqing Yang, Lili Qiu, and Yang You. 2025. SortedRL: Accelerating RL Training for LLMs through Online Length-aware Scheduling. In *ES-FoMo III: 3rd Workshop on Efficient Systems for Foundation Models*. <https://openreview.net/forum?id=YoV9lIZ827>

[54] Yinmin Zhong, Zili Zhang, Xiaoniu Song, Hanpeng Hu, Chao Jin, Bingyang Wu, Nuo Chen, Yukun Chen, Yu Zhou, Changyi Wan, Hongyu Zhou, Yimin Jiang, Yibo Zhu, and Dixin Jiang. 2025. StreamRL: Scalable, Heterogeneous, and Elastic RL for LLMs with Disaggregated Stream Generation. (2025). arXiv:cs.LG/2504.15930 <https://arxiv.org/abs/2504.15930>

[55] Yinmin Zhong, Zili Zhang, Bingyang Wu, Shengyu Liu, Yukun Chen, Changyi Wan, Hanpeng Hu, Lei Xia, Ranchen Ming, Yibo Zhu, and Xin Jin. 2025. Optimizing RLHF Training for Large Language Models with Stage Fusion. In *22nd USENIX Symposium on Networked Systems Design and Implementation (NSDI 25)*. USENIX Association, Philadelphia, PA, 489–503. <https://www.usenix.org/conference/nsdi25/presentation/zhong>

[56] Yuzhen Zhou, Jiajun Li, Yusheng Su, Gowtham Ramesh, Zilin Zhu, Xiang Long, Chenyang Zhao, Jin Pan, Xiaodong Yu, Ze Wang, Kanggrui Du, Jialian Wu, Ximeng Sun, Jiang Liu, Qiaolin Yu, Hao Chen, Zicheng Liu, and Emad Barsoum. 2025. APRIL: Active Partial Rollouts in Reinforcement Learning to Tame Long-tail Generation. (2025). arXiv:cs.LG/2509.18521 <https://arxiv.org/abs/2509.18521>